Quasielastic backscattering and barrier distribution for the weakly bound projectile ^{6}Li on ^{159}Tb

Piyasi Biswas,[1,3,*] A. Mukherjee,[1,3,†] Saikat Bhattacharjee,[1,3] D. Chattopadhyay,[2,‡] Subinit Roy,[1] S. Santra,[2,3] S. K. Pandit,[2] K. Ramachandran,[2] K. Mahata,[2,3] and A. Shrivastava[2,3]

[1]*Saha Institute of Nuclear Physics, 1/AF Bidhannagar, Kolkata 700064, India*

[2]*Nuclear Physics Division, Bhabha Atomic Research Centre, Mumbai 400085, India*

[3]*Homi Bhabha National Institute, Anushaktinagar, Mumbai 400094, India*

(Received 8 April 2021; revised 25 June 2021; accepted 23 August 2021; published 20 September 2021)

The excitation function for quasielastic scattering of the weakly bound projectile ^{6}Li on a ^{159}Tb target, at large backward angle, has been measured at energies around the Coulomb barrier. The corresponding quasielastic barrier distribution has been extracted from the experimental cross sections, both including and excluding the α particles produced in the reaction. The quasielastic scattering cross sections, excluding the α particles, have been analyzed in the framework of coupled channels calculations. The centroid of the quasielastic barrier distribution, including the α particles, is found to shift towards higher energy relative to the centroid of the fusion barrier distribution for the system. This has been attributed to the low α-breakup threshold of the nucleus ^{6}Li.

DOI: 10.1103/PhysRevC.104.034620

I. INTRODUCTION

Large back-angle quasielastic scattering is a powerful tool for the analysis of barrier distributions close to the Coulomb barrier [1]. Investigation of the quasielastic scattering process in various systems has been stimulated in recent years, especially in the context of reactions induced by weakly bound stable projectiles, where breakup is an important reaction mechanism. Quasielastic (QEL) scattering is defined as the sum of all direct processes, like elastic and inelastic scattering and transfer channels. Large back-angle QEL scattering is complementary to the fusion process, since the former is related to the reflection probability at the barrier, while the latter is related to the penetration probability.

Fusion is usually the dominant mode of reaction at energies around the barrier, except in cases where direct reaction channels dominate at lower energies. It is well known that the coupling of the relative motion of the colliding nuclei to their internal degrees of freedom manifests itself as a strong enhancement of fusion cross sections at sub-barrier energies [2]. However, the nature of the couplings affecting the fusion process is not always apparent from the measured fusion excitation function. Rowley *et al.* [3] proposed that a barrier distribution, resulting from channel couplings, can be extracted from a precisely measured fusion excitation function using the relation

$$D_{\rm fus}(E) = \frac{d^2}{dE^2}[E\sigma_{\rm fus}(E)], \tag{1}$$

where $\sigma_{\rm fus}(E)$ is the fusion cross section for the system at the center-of-mass energy E. Over the years, this prescription has been very successful for understanding the fusion mechanism in a wide range of reactions [2].

Alternatively, a similar barrier distribution can also be extracted from a much simpler measurement of the QEL scattering excitation function at large back angle. The QEL barrier distribution $D_{\rm qel}$ is obtained as [4]

$$D_{\rm qel}(E) = -\frac{d}{dE}\left[\frac{d\sigma_{\rm qel}}{d\sigma_{\rm Ruth}}(E)\right], \tag{2}$$

where $(d\sigma_{\rm qel}/d\sigma_{\rm Ruth})$ is the ratio of QEL scattering and Rutherford scattering differential cross sections at a fixed back angle. Zagrebaev [5] argued that the barrier distribution obtained from QEL scattering excitation function determines a threshold distribution for all reaction processes other than fusion, and this has important ramifications in the case of heavy or weakly bound projectiles, where contributions from deep-inelastic collisions or breakup processes are important. This interpretation explains the differences observed in the distributions obtained from fusion and QEL scattering for very heavy systems, like ^{48}Ti + ^{208}Pb, ^{64}Ni + ^{208}Pb, and ^{70}Zn + ^{208}Pb [6], where the deep-inelastic process is a significant contributor. A similar situation can also arise in the case of reactions with weakly bound nuclei, where the breakup channel is an important reaction mechanism.

For weakly bound nuclei, following projectile breakup if none of the fragments are captured by the target then the process is called noncapture breakup (NCBU); if one of the fragments fuses with the target then it is called an incomplete fusion (ICF) process. The breakup channel is known to

*Present address: Shahid Matangini Hazra Government College for Women, Tamluk, Chakshrikrishnapur, Kulberia, Purba Medinipur, West Bengal 721649, India.

†anjali.mukherjee@saha.ac.in

‡Present address: Tata Institute of Fundamental Research, Mumbai 400005, India.

affect the fusion process considerably [7]. While comparing complete fusion $D_{\rm fus}$ for weakly bound nuclei with the corresponding $D_{\rm qel}$, whether or not the breakup process should be considered in QEL events has remained a puzzle for several years now. Barrier distributions have been derived from large back-angle QEL scattering measurements for various weakly bound systems [8–19], but $D_{\rm qel}$ has been compared with $D_{\rm fus}$ only for a few systems [8,13–15,18–21]. For systems where breakup related nonfusion channels dominate over fusion, the distribution $D_{\rm qel}$ appears to be broader and shifted towards lower energy compared to $D_{\rm fus}$. For the system ^{6}Li + ^{64}Ni, $D_{\rm qel}$ was observed to be peaked at an energy 450 keV lower compared to the peak of $D_{\rm fus}$ [19]. Lin *et al.* [8] compared $D_{\rm fus}$ and $D_{\rm qel}$ for ^{6,7}Li + ^{208}Pb and observed a strong shift in the peak of $D_{\rm qel}$ to a lower energy compared to $D_{\rm fus}$. However, on inclusion of the contribution of α particles in the definition of QEL events, $D_{\rm qel}$ agrees reasonably with $D_{\rm fus}$ for both the systems. For the systems ^{6,7}Li + ^{197}Au, Palshetkar *et al.* [18] observed that the centroid of $D_{\rm qel}$, obtained after inclusion of the α-particle contribution to the QEL events, was shifted towards a higher energy compared to that of $D_{\rm fus}$, while the centroid of $D_{\rm qel}$, excluding the contribution of the α particles, was shifted towards a lower energy with respect to $D_{\rm fus}$. By contrast, for ^{7}Li + ^{159}Tb it was recently reported that the centroid of $D_{\rm qel}$, after inclusion of the breakup α particles, agrees with that of $D_{\rm fus}$ [21]. In the context of this conflicting scenario, it seems worthwhile to investigate $D_{\rm qel}$ for the reaction induced by the weakly bound stable projectile ^{6}Li on the target ^{159}Tb and compare it with the corresponding $D_{\rm fus}$.

Therefore, a measurement of the large back-angle QEL scattering excitation function was carried out for the system ^{6}Li + ^{159}Tb and the corresponding barrier distribution was derived using Eq. (2). To study the influence of ^{6}Li and ^{159}Tb inelastic excitations on the QEL scattering process, coupled channels calculations have been done. Complete and incomplete fusion excitation functions for the same system at near-barrier energies were reported earlier in Ref. [22]. The QEL barrier distribution for the system determined in this work has been compared with the fusion barrier distribution extracted from the complete fusion cross sections of Ref. [22].

II. EXPERIMENTAL DETAILS

The experiment was carried out at the 14UD BARC-TIFR Pelletron-Linac Facility in TIFR, Mumbai, India. A self-supporting ^{159}Tb target foil of thickness ≈560 μg/cm^2 was bombarded by beams of ^{6}Li, in the energy range $E_{\rm lab}$ = 17–33 MeV. The beam energy was varied in steps of 1 MeV at energies well below and well above the Coulomb barrier. Beam currents varied from 7 to 28 nA. The incident beam energies were corrected for the loss of energy in the target material at half thickness of the target. A set of four silicon ΔE-E telescopes, mounted at ±170° and ±160° inside a scattering chamber of diameter 1 m, was used to detect and identify the charged particles produced in the reaction. The thicknesses of the detectors of each telescope were chosen that the charged particles lose part of their kinetic energies in the first detector (ΔE) and stop by depositing the residual energies ($E_{\rm res}$) in the second detector (E). However, none of the stop detectors was thick enough to stop the Z = 1 particles. Two Si-surface barrier detectors, each of thickness 300 μm, were placed at ±20° relative to the beam direction for monitoring the beam and also for normalization purposes. A collimator was placed in front of each telescope and monitor to define the solid angle. The data acquisition system LAMPS [23] was used for data recording and analysis. The solid angle ratios between the monitors and telescopes were determined by bombarding a gold target at low beam energies, for which the elastic scattering cross section was purely Rutherford.

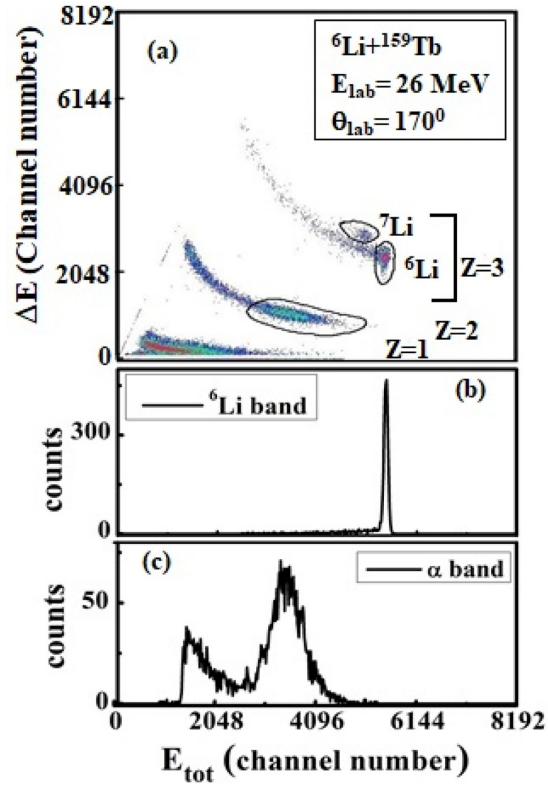

FIG. 1. (a) A typical ΔE-$E_{\rm tot}$ spectrum for the ^{6}Li + ^{159}Tb reaction at $E_{\rm lab}$ = 26 MeV and laboratory scattering angle $\theta_{\rm tel}$ = 170°. The areas defined by the solid lines represent the events used in the respective bands for determining the cross sections corresponding to different reaction processes. Also shown are the one-dimensional projections for (b) ^{6}Li and (c) Z = 2 bands.

III. DATA ANALYSIS AND RESULTS

Figure 1(a) shows a typical two-dimensional ΔE-$E_{\rm tot}$ (where $E_{\rm tot} = \Delta E + E_{\rm res}$) spectrum measured at $E_{\rm lab}$ = 26 MeV and laboratory scattering angle of 170°. Events corresponding to Z = 1, 2, and 3 can be seen to be well separated. The enclosed areas marked on the Z = 3 and Z = 2 bands in the figure represent the different integration areas used in determining the cross sections of the respective reaction processes. The Z = 3 band has two components: ^{6}Li and ^{7}Li. The ^{6}Li band primarily consists of contributions from elastic and inelastic scattering events. The events corresponding to the inelastically scattered excited states of ^{159}Tb could not be

TABLE I. Ground state Q values, Q_{gg}, and optimum Q values, $Q_{\rm opt}$, for different transfer channels, in the reaction ^{6}Li + ^{159}Tb. The $Q_{\rm opt}$ values have been calculated at two typical energies, $E_{\rm c.m.} = 22$ and 25 MeV.

Transfer channel	Q_{gg} (MeV)	$Q_{\rm opt}$ (MeV)
	$E_{\rm c.m.} = 22$ MeV	
n stripping	+0.71	0
n pickup	−0.88	0
p stripping	+3.00	−7.11
p pickup	−0.52	+6.88
d stripping	+10.18	−7.11
d pickup	+10.44	+6.88
	$E_{\rm c.m.} = 25$ MeV	
n stripping	+0.71	0
n pickup	−0.88	0
p stripping	+3.00	−8.08
p pickup	−0.52	+7.82
d stripping	+10.18	−8.08
d pickup	+10.44	+7.82

separated from the elastic scattering events, because of the closely spaced low-lying levels of ^{159}Tb. The ΔE detector resolution was good enough to separate ^{7}Li from ^{6}Li events and so in the spectrum one can see a separate blob of ^{7}Li events, arising from the n-pickup process, just above the elastic scattering band. Figure 1(b) shows the one-dimensional projection of the ^{6}Li band.

The $Z = 2$ band consists of α particles produced via different processes in the reaction. Figure 1(c), the one-dimensional projection of the $Z = 2$ band, shows a broad, continuous α peak, with centroid around two-thirds of the beam energy, corresponding to the marked region in Fig. 1(a). The events in this broad peak mainly originate from breakup related processes, like no-capture breakup ($\alpha + d$) of ^{6}Li, d capture by the target following breakup of ^{6}Li (and/or d stripping) and breakup following p-stripping, n-stripping, and/or n-pickup processes [24–26]. The n-pickup process may yield α particles, if the resulting ^{7}Li nucleus is produced at energies above its α breakup threshold and breaks into α and t. The ground state Q values, Q_{gg}, and optimum Q values, $Q_{\rm opt}$, corresponding to different transfer channels that can contribute to the broad α peak are shown in Table I. The energy dependent $Q_{\rm opt}$ values have been calculated [27] at two typical energies, $E_{\rm c.m.} = 22$ and 25 MeV. Transfer reactions preferentially populate final states with excitation energies around, $\epsilon^{*} = Q_{gg}$-$Q_{\rm opt}$. It may be expected that the breakup of nulceus ^{7}Be, following the p-pickup process may produce α particles, but from Q-value consideration (see Q_{gg} and $Q_{\rm opt}$ values in Table I), such a process seems to be energetically unfavorable. The d-pickup process producing ^{8}Be, which immediately breaks into two α particles, will also contribute to the broad α peak, but the contribution from this channel is expected to be very small in the ^{6}Li + ^{159}Tb reaction, as compared to the total contribution to α particles from other processes [26]. The low energy background region of the α-particle band in the spectrum arises primarily due to the target impurities, like ^{12}C and ^{16}O [28,29]. A statistical model calculation done using the code PACE [30] shows that the contribution of compound nucleus evaporation α particles in this reaction is negligibly small, and the compound nucleus decays predominantly by xn channels [22]. The contribution from evaporation α particles in the low energy part of the α particle band is therefore expected to be insignificant.

The events corresponding to $Z = 1$ could not be used in the analysis, as the E detectors were not thick enough to stop the $Z = 1$ particles. We refer to the $Z = 3$ band as "partial" QEL events because it does not correspond to the full QEL scattering cross section, which would include all relevant reaction channels. The x axis of the two-dimensional ΔE-$E_{\rm tot}$ spectra in Fig. 1 was energy calibrated using the elastic peaks of ^{6}Li projectile scattered from the ^{159}Tb target, at different incident energies below the Coulomb barrier. The QEL scattering excitation function was obtained by using the expression

$$\frac{d\sigma_{\rm qel}}{d\sigma_{\rm Ruth}}(E,\theta_{\rm tel}) = \left[\frac{N_{\rm qel}(E,\theta_{\rm tel})}{N_m(E,\theta_m)}\right] \times \left[\frac{(d\sigma_{\rm Ruth}/d\Omega)(E,\theta_m)}{(d\sigma_{\rm Ruth}/d\Omega)(E,\theta_{\rm tel})}\right]\left(\frac{\Delta\Omega_m}{\Delta\Omega_{\rm tel}}\right), \quad (3)$$

where $N_{\rm qel}$ is the yield in the telescope detector, N_m is the average yield in the two monitor detectors, and $\frac{d\sigma_{\rm Ruth}}{d\Omega}(E,\theta_m(\theta_{\rm tel}))$ is the calculated Rutherford scattering cross section at the corresponding bombarding energy E and monitor angle θ_m (telescope angle $\theta_{\rm tel}$). The factor $\frac{\Delta\Omega_m}{\Delta\Omega_{\rm tel}}$ is the solid angle ratio of monitor to telescope detector. The $\frac{\Delta\Omega_m}{\Delta\Omega_{\rm tel}}$ ratio was determined from the measurements at the lowest bombarding energies of 17, 18, and 19 MeV, where the elastic scattering is purely Rutherford. The ratio was estimated to be 0.00500 ± 0.00004. As the detectors were placed at angles less than 180°, centrifugal correction was incorporated to estimate the effective c.m. energies ($E_{\rm eff}$). The results of QEL events at ±170° and ±160° were converted to those for 180° by mapping to $E_{\rm eff}$ using the relation [4]

$$E_{\rm eff} = \frac{2E_{\rm c.m.}}{1 + \csc(\theta_{\rm c.m.}/2)} \quad (4)$$

The good agreement between the QEL excitation functions and barrier distributions, extracted using the data taken at ±170° and ±160°, after appropriate centrifugal correction, confirmed the consistency of our experimental data. The "partial" QEL excitation function determined from only ^{6}Li events and the corresponding barrier distribution, $D_{\rm qel}$, extracted using Eq. (2) are shown by the solid squares in Figs. 2(a) and 2(b), respectively. The solid triangles in the figures show the "partial" QEL excitation function obtained from the summed contributions of elastic, inelastic, and n-pickup (^{7}Li) events and the corresponding $D_{\rm qel}$. However, the contribution of the n-pickup channel in the QEL excitation function is found to be significantly small. According to Zagrebaev, if breakup related processes are not included in the QEL events, the QEL barrier distribution represents the reaction threshold distribution [5]. Hence, the partial $D_{\rm qel}$ extracted from the $Z = 3$ events only and shown in Fig. 2(b) by the solid triangles, does

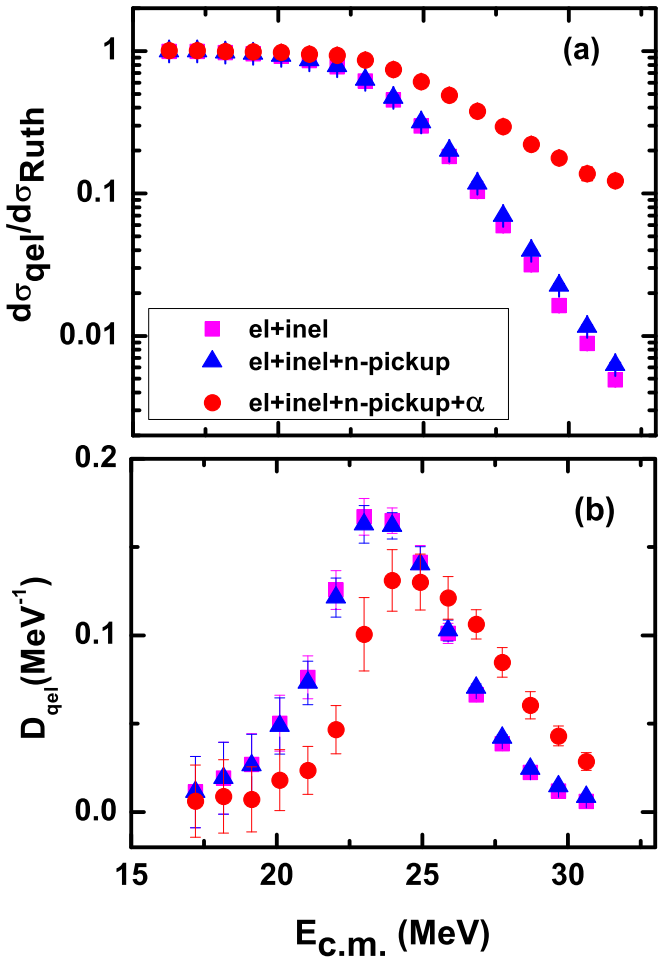

FIG. 2. Comparison of (a) quasielastic excitation function and (b) quasielastic barrier distribution for ^{6}Li + ^{159}Tb, excluding and including α particles.

not correspond to the fusion barrier distribution, but rather reflects the reaction threshold distribution. The QEL scattering excitation function and the corresponding $D_{\rm qel}$, obtained from the sum of $Z = 3$ (elastic + inelastic + n pickup) and $Z = 2$ (α) events are also plotted in Figs. 2(a) and 2(b), by the solid circles. It can be seen that inclusion of the contribution of the α particles in the definition of QEL events shifts the peak of $D_{\rm qel}$ to higher energy by $\approx$1 MeV and also broadens the distribution.

IV. COUPLED CHANNELS CALCULATIONS

To investigate the effects of couplings between different reaction channels, the measured "partial" QEL excitation function and the corresponding barrier distribution have been analyzed using the coupled channels code FRESCO (version FRES 2.9) [31]. The calculations have been performed for $Z = 3$ events only, because as discussed above it was not possible to distinguish clearly the different reaction channels contributing to $Z = 2$ events, in the present inclusive measurement.

TABLE II. Reduced transition probabilities $B(E2)$ [35] used in the coupled channels analysis to calculate the transition matrix elements and nuclear deformation lengths for excited states states in ^{159}Tb

Transition $(J_i \rightarrow J_f)$	$B(E2; J_i \rightarrow J_f)$ (e^2b^2)
$5/2 \rightarrow 3/2$	1.87
$7/2 \rightarrow 5/2$	1.25
$7/2 \rightarrow 3/2$	0.72
$9/2 \rightarrow 7/2$	0.61
$9/2 \rightarrow 5/2$	1.13
$11/2 \rightarrow 9/2$	0.56
$11/2 \rightarrow 7/2$	1.47

To perform the coupled channels (CC) calculations, one needs the entrance channel optical potential which consists of the Coulomb potential and bare nuclear potential with real and imaginary parts. In the calculations, the Coulomb potential was assumed to be that of a uniformly charged sphere with radius $R_C = r_C(A_P^{1/3} + A_T^{1/3})$, where A_P and A_T are the mass numbers of projectile and target, respectively, and r_C is the radius parameter which was considered to be 1.3 fm. The real part of the bare nuclear potential was considered to be a double-folding (DF) potential, that was generated using the density dependent M3Y-Reid (DDM3Y) nucleon-nucleon interaction with an energy independent zero-range exchange term [32]. The density dependence of the interaction was taken from Ref. [33]. The matter density for ^{6}Li was derived from the charge distribution by assuming similar shapes for both proton and neutron distributions. The proton distribution of ^{6}Li was obtained by using the parametric form for charge distribution from Ref. [32]. The matter density for ^{159}Tb was obtained from Ref. [34]. The imaginary part of the bare potential was taken to be of Woods-Saxon shape with depth, radius, and diffuseness parameters values $W_0 = 50.0$ MeV, $r_w = 1.0$ fm, $a_w = 0.3$ fm, respectively. The short range of the imaginary potential simulates the ingoing-wave boundary condition for the core fusion process.

The CC calculations were performed by coupling the four low-lying collective states of the target ^{159}Tb: $5/2^+$ at 0.058 MeV, $7/2^+$ at 0.137 MeV, $9/2^+$ at 0.240 MeV and $11/2^+$ at 0.365 MeV. The form factors were chosen to be derivatives of the undeformed potential. To obtain the transition potentials for the inelastic channels, the entrance channel potential was deformed with coupling strengths determined from the respective reduced transition probabilities, $B(E2)$ values. The $B(E2)$ values for the corresponding transitions in ^{159}Tb used [35] in the calculations are listed in Table II. The Coulomb matrix elements and the nuclear deformation lengths for the inelastic transitions were derived from the $B(E2)$ values, assuming a rotational model for ^{159}Tb. The QEL excitation function thereby calculated is compared with the experimental excitation function in Fig. 3. The corresponding barrier distribution is plotted in Fig. 4. In the present experiment, the inelastically scattered events could not be separated from the elastic events because of the closely spaced

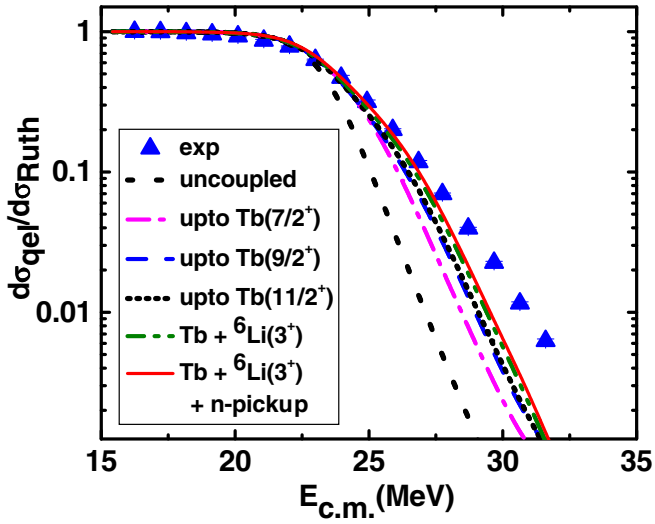

FIG. 3. Comparison of experimental quasielastic excitation function with the FRESCO calculations for the system ^{6}Li + ^{159}Tb. See text for details.

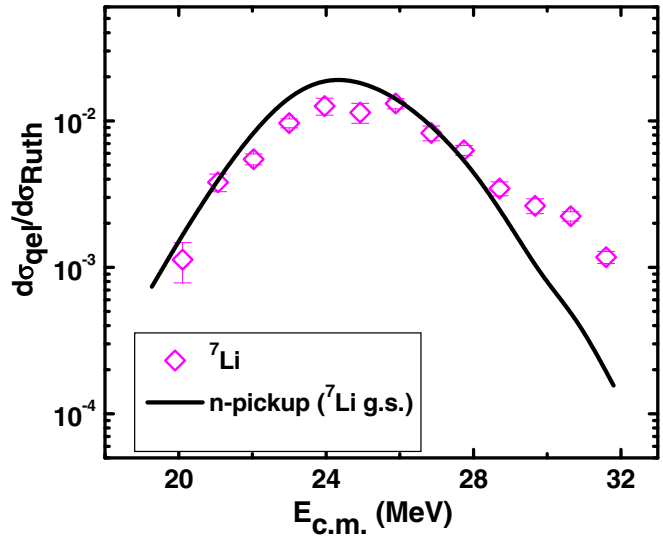

FIG. 5. Comparison of the measured ^{7}Li production cross sections in the ^{6}Li + ^{159}Tb reaction with the DWBA calculations. See text for details.

low-lying levels of ^{159}Tb. For comparison with experimental results, the calculated QEL scattering cross sections were determined by adding the calculated elastic cross sections to the cross sections corresponding to the inelastic states of ^{159}Tb. The no-coupling calculations are shown by the dotted lines in the figures. The dot-dashed and dashed lines show the coupled channels calculations with couplings up to the $7/2^+$ state and up to $9/2^+$ state of ^{159}Tb, respectively. The short dotted lines in Figs, 3 and 4 show the results obtained after including inelastic coupling up to $11/2^+$ state in the target ^{159}Tb. Inclusion of coupling to the next higher excited state of $13/2^+$ at 0.51 MeV produced no significant effect. It is observed that inelastic coupling to excited states of ^{159}Tb leads to enhancement of cross sections at higher energies compared to uncoupled calculations; but agreement with the experimental data is still poor.

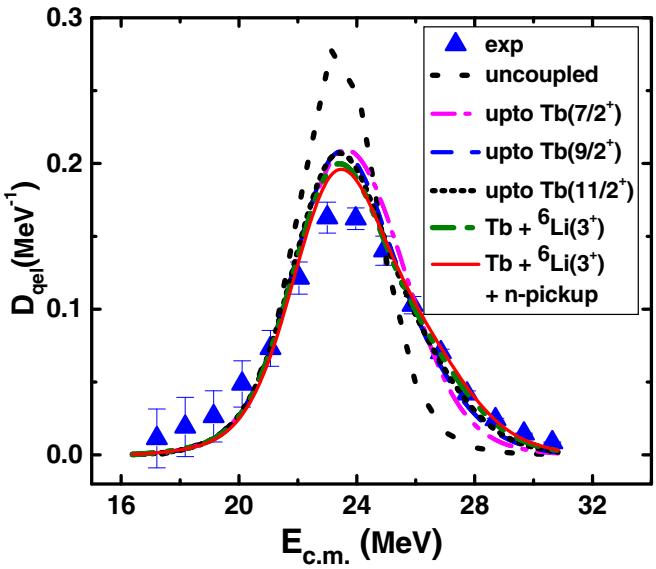

FIG. 4. Comparison of the experimental quasielastic barrier distribution with the FRESCO calculations for the system ^{6}Li + ^{159}Tb. See text for details.

The 3^+ resonant excited state of the ^{6}Li projectile at 2.18 MeV was then included in the CC calculations. The reduced transition probability $B(E2)$ for the transition from the ground state to the 3^+ (2.18 MeV) state in ^{6}Li was taken to be 25.6 e^2fm^4 [36]. The Coulomb matrix element was determined from the $B(E2)$ value by assuming a rotational model. Reorientation couplings were also considered in the calculations. The calculations thereby obtained are compared with the experimental data in Figs. 3 and 4 by the dot-dot-dashed lines. Note that the calculated QEL cross sections shown by the dot-dot-dashed lines do not include the inelastic cross sections corresponding to the 3^+ resonant state of ^{6}Li. It is observed that inclusion of the 3^+ resonant state of ^{6}Li in the coupling scheme shows significant changes in both QEL excitation function and barrier distribution, but the agreement with data is still poor.

Thus we see that coupling to the lower lying excited states of ^{159}Tb enhances the QEL cross sections at higher energies along with broadening of the barrier distribution and reduction in the height of the distribution, compared to the no-coupling calculations. Including the 3^+ resonant state of ^{6}Li, corresponding to sequential breakup in the coupling scheme, improves the excitation function and barrier distribution, but agreement with experimental data is still far away.

As already mentioned above, ^{7}Li events originating due to n pickup by the ^{6}Li projectile appear just above the ^{6}Li band. The production of ^{7}Li nuclei in Fig. 1 via compound nucleus evaporation is invalidated by a statistical model calculation [22]. The n-pickup cross sections corresponding to the ^{7}Li events are plotted in Fig. 5. In order to compare the experimental n-pickup cross sections with theory, an attempt was made to calculate the cross sections for the n-pickup

process to populate the g.s. $(3/2^-)$. The n-pickup cross sections were calculated in the framework of the distorted wave Born approximation (DWBA) at different bombarding energies around the Coulomb barrier for the ^{6}Li + ^{159}Tb system. For the ^{6}Li + ^{158}Tb core-core interaction and the exit channel ^{7}Li + ^{158}Tb, the global optical model potential parameters of Ref. [37] were used. The required binding potentials for n-^{6}Li and n-^{158}Tb were taken from Refs. [38,39], respectively. The depth was adjusted to reproduce the neutron binding energy to the core nucleus. For the ^{6}Li (g.s.) : ^{7}Li (g.s.) overlap, the spectroscopic factors (SFs) for $1p_{3/2}$ and $1p_{1/2}$ orbitals were taken to be 0.735 and 0.657 [40], respectively. As the neutron SFs to the g.s. and 0^- state of ^{158}Tb are unavailable in the literature, the SF for ^{159}Tb : ^{158}Tb + n is taken to be 1. Finite range DWBA calculations have been done using the prior form of interaction. The cross sections thereby calculated are shown by solid lines and compared with the n-pickup data in Fig. 5. The shapes of the experimental and theoretical excitation functions are found to be in reasonable agreement, barring a few high energy points. These high energy points could not be reproduced even after including the first bound $1/2^-$ state of ^{7}Li in the calculations. Inclusion of the first bound $1/2^-$ state along with the g.s. of ^{7}Li in the calculations did not show any significant change in shape of the excitation function other than an overall increase of the cross sections and therefore has not been considered further in this paper.

To probe the effect of n-pickup coupling on the QEL excitation function and barrier distribution, coupled reaction channels (CRC) calculations were done, including couplings to the n-pickup channel leading to the g.s. of ^{7}Li, in addition to the inelastic couplings described above. The resulting CRC calculations are shown by the solid lines in Figs. 3 and 4. Inclusion of n-pickup coupling slightly increases the QEL scattering cross sections at higher energies, but has no significant effect on the barrier distribution. The effect of coupling to n pickup leading to the first bound $1/2^-$ state of ^{7}Li was also found to be insignificant and therefore has not been shown in the figures. Thus we see that the coupling to the lower lying excited states of ^{159}Tb, the 3^+ resonant state of ^{6}Li, and the n-pickup channel could not give a satisfactory description of the measured QEL excitation function and barrier distribution.

The n-stripping process, with $Q_{gg} = +0.71$ MeV, is an important channel in the ^{6}Li + ^{159}Tb reaction, that results in a considerable fraction of α particles, following the breakup of the unstable ^{5}Li nucleus [26]. Though this channel will not contribute to the "partial" QEL cross sections, corresponding to $Z = 3$ considered here, coupling to this channel may be expected to influence the elastic cross sections and hence affect the "partial" QEL cross sections. The CRC calculations were therefore done including coupling to the n-stripping channel to produce the g.s. and first excited state of ^{160}Tb, taking SFs to be 1 for the two states, in addition to the inelastic and n-pickup couplings, but were found to show no significant effect on the "partial" QEL excitation function and barrier distribution. As Q_{gg} for n stripping is +0.710 MeV, n transfer to produce higher excited states of ^{160}Tb is expected to be favored. But due to the unavailability of proper SFs for the excited states of ^{160}Tb (:^{159}Tb + n), further calculations including coupling to the n-stripping channel were not carried out.

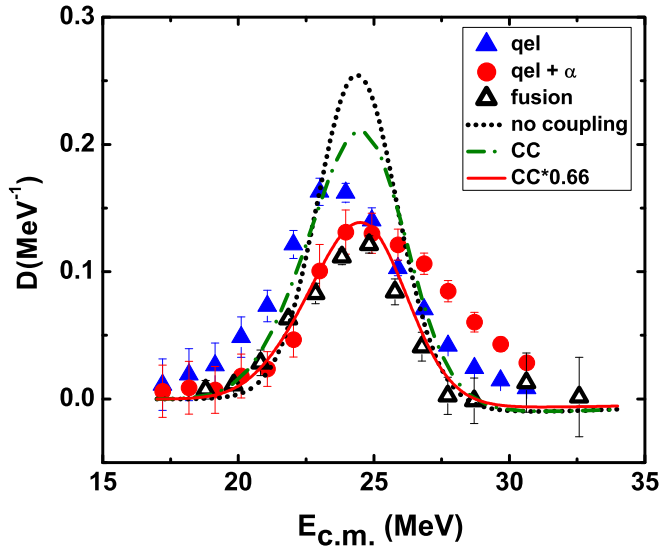

FIG. 6. Comparison of the barrier distributions obtained from the QEL excitation function, excluding and including α particles, with the CF barrier distribution for the system ^{6}Li + ^{159}Tb. The $D_{\rm fus}$ values have been normalized by the factor $1/(\pi R_b^2)$ to compare with $D_{\rm qel}$. See text for details.

The discrepancies observed between theoretical predictions and experimental results for excitation functions and corresponding barrier distributions might be attributed to the effects of the channels not taken into account in the coupling scheme, such as transfer processes not considered here and direct breakup reactions. For ^{6}Li induced reactions, breakup related channels are expected to be important due to the low breakup threshold of 1.47 MeV for $\alpha + d$ breakup. For the ^{6,7}Li + ^{59}Co reactions at near-barrier energies [41], the calculations indicate that although the breakup cross sections are a small fraction of the total reaction cross sections, coupling to the breakup channel has a significant effect on the elastic scattering. Luong *et al.* [42] showed that for ^{6,7}Li + ^{208}Pb reactions the breakup following transfer is the dominant breakup mechanism at sub-barrier energies. Thus other reaction channels not included in our coupled channels calculations (like direct breakup and/or transfer) might be needed for better agreement between experimental data and theoretical results.

V. COMPARISON OF $D_{\rm qel}$ AND $D_{\rm fus}$

To investigate the importance of α-particle contribution in defining QEL scattering events for ^{6}Li-induced reactions, the distributions $D_{\rm qel}$ for ^{6}Li + ^{159}Tb, both including and excluding the α particles, have been compared with the $D_{\rm fus}$ for the system in Fig. 6. The distribution $D_{\rm fus}$ has been extracted from the reported CF cross sections [22,43] by using expression (1) and is shown by open triangles in the figure. Error bars in $D_{\rm fus}$ were calculated from statistical errors in the CF cross sections. For comparing the two distributions, $E_{\rm step}$ was taken

to be 2 MeV for both the cases. To compare $D_{\rm qel}$ with $D_{\rm fus}$, the $D_{\rm fus}$ values were normalized by $1/\pi R_b^2$, where R_b is the barrier radius, taken from Ref. [22]. The different curves in the figure correspond to $D_{\rm fus}$ extracted from the coupled channels calculated cross sections, using the code CCFULL [44] and the coupling scheme and potential as mentioned in Ref. [22]. The dotted curve represents the no-coupling calculations. The dot-dashed curve represents the coupled channels calculations using target inelastic excitations, following Ref. [22]. As the CF cross sections were found to be suppressed by a factor of 0.66 for the reaction ^{6}Li + ^{159}Tb [22], the solid curve was obtained by extracting CF $D_{\rm fus}$ from the coupled channels calculated cross sections scaled by a factor of 0.66. The solid curve is seen to reproduce reasonably well the experimental CF $D_{\rm fus}$ for the system.

It can be observed from the figure that the $D_{\rm qel}$ derived from the sum of elastic, inelastic, and n-pickup events is broader and the centroid of the distribution is shifted towards lower energy by about 1.2 MeV compared to that of $D_{\rm fus}$. Similar energy shift was also reported for the system, ^{6}Li + ^{144}Sm [45]. However, a smaller energy shift of 450 keV was reported for the medium mass system ^{6}Li + ^{64}Ni. This result is consistent with the interpretation of Zagrebaev [5] that the barrier distribution obtained from QEL scattering measurement represents the total reaction threshold distribution, which will reflect in the difference in the barrier distributions obtained from CF and QEL excitation functions. It was conjectured that, for systems where breakup related nonfusion channels dominate over fusion, if breakup related processes are not included in the QEL events, the centroid of the $D_{\rm qel}$ should be shifted to the low-energy side when compared with the CF $D_{\rm fus}$.

From the figure, it can also be seen that the inclusion of α particles in the QEL events shifts the peak of the distribution $D_{\rm qel}$ towards higher energy such that the position of the maximum of the distribution matches reasonably well with that of the CF $D_{\rm fus}$. However, the distribution $D_{\rm qel}$, including the α particles, is broader than $D_{\rm fus}$, which results in a shift of the centroid of the distribution $D_{\rm qel}$ towards higher energy compared to that of $D_{\rm fus}$. A similar feature has also been observed for the system ^{6}Li + ^{197}Au [18]. However, this contradicts the observations reported for ^{7}Li + ^{159}Tb [21] and ^{6,7}Li + ^{208}Pb [8] systems.

The disagreement between the centroids of the two distributions, $D_{\rm qel}$, including the α-particle contribution, and $D_{\rm fus}$ in ^{6}Li + ^{159}Tb reaction might be understood in the following way. Since fusion and back-angle QEL scattering are complementary, it follows that

$$1 - \sigma_{\rm fus} = \sigma_{\rm qel}, \tag{5}$$

where $\sigma_{\rm fus}$ and $\sigma_{\rm qel}$ are fusion and QEL scattering cross sections, respectively. For ^{6}Li induced reactions,

$$\sigma_{\rm fus} = \sigma_{\rm CF} + \sigma_{\rm ICF}, \tag{6}$$

where $\sigma_{\rm CF}$ and $\sigma_{\rm ICF}$ are CF and ICF cross sections, respectively. Also,

$$\sigma_{\rm ICF} = \sigma_{\alpha\text{-ICF}} + \sigma_{d\text{-ICF}}. \tag{7}$$

Here, $\sigma_{\alpha\text{-ICF}}$ and $\sigma_{d\text{-ICF}}$ are the ICF processes where α and d are captured by the target, respectively. It needs to be noted here that for ^{6}Li + ^{159}Tb, measured $\sigma_{d\text{-ICF}}$ also includes d transfer to ^{159}Tb, if any [22]. Also, in this reaction, the d-capture (and/or d-stripping) process where an α particle is emitted is the dominant ICF contributor compared to the less favored α-capture process [22]. Therefore, $\sigma_{\rm ICF} \approx \sigma_{d\text{-ICF}}$. Eq. (5) may then be written as

$$1 - (\sigma_{\rm CF} + \sigma_{d\text{-ICF}}) = \sigma_{el+\rm inel} + \sigma_{n\text{-pickup}} + \sigma_{n\text{-strip}} + \sigma_{p\text{-strip}}, \tag{8}$$

where $\sigma_{el+\rm inel}$, $\sigma_{n\text{-pickup}}$, $\sigma_{n\text{-strip}}$ and $\sigma_{p\text{-strip}}$ are the cross sections corresponding to the sum of elastic and inelastic events, n-pickup, n-stripping, and p-stripping reactions, respectively. The contribution to QEL cross sections corresponding to d stripping is not written explicitly on the right-hand side of the equation because the d-stripping cross section is already included in $\sigma_{d\text{-ICF}}$. On the right-hand side of this equation, contributions from two channels, namely $\sigma_{p\text{-pickup}}$ and $\sigma_{d\text{-pickup}}$, have been omitted here. It has already been discussed in Sec. III that the p-pickup process is energetically unfavorable and the contribution to α particles from the d-pickup process is expected to be very small in the ^{6}Li + ^{159}Tb reaction.

Equation (8) then yields

$$1 - \sigma_{\rm CF} = \sigma_{d\text{-ICF}} + \sigma_{\rm qel}^{\rm meas} + \sigma_{n\text{-strip}} + \sigma_{p\text{-strip}}, \tag{9}$$

where $\sigma_{\rm qel}^{\rm meas}$ is the measured QEL scattering cross sections corresponding to the sum of elastic, inelastic, and n-pickup events. The α-particle events used (marked in Fig. 1) to calculate the corresponding contribution primarily originate from d-ICF, breakup, and transfer induced breakup processes. Therefore, the dominant contributions to the inclusive α particles can be written as

$$\sigma_{\alpha\text{-incl}} = \sigma_{\alpha\text{-}d} + \sigma_{d\text{-ICF}} + \sigma_{n\text{-strip}} + \sigma_{p\text{-strip}}. \tag{10}$$

Here, $\sigma_{\alpha\text{-incl}}$ is the measured inclusive α cross sections and $\sigma_{\alpha\text{-}d}$ represents the α cross sections corresponding to direct and sequential breakup of ^{6}Li. Comparison of Eqs. (9) and (10) gives

$$1 - \sigma_{\rm CF} = \sigma_{\rm qel}^{\rm meas} + (\sigma_{\alpha\text{-incl}} - \sigma_{\alpha\text{-}d}). \tag{11}$$

For ^{6}Li + ^{159}Tb, the ^{6}Li-breakup contribution, $\sigma_{\alpha\text{-}d}$, though small compared to total $\sigma_{\alpha\text{-incl}}$ [22], cannot be neglected, unlike the case of ^{7}Li + ^{159}Tb where $\sigma_{\alpha\text{-}t}$ can be neglected [21]. This is because the ^{6}Li nucleus has a lower α-breakup threshold compared to the nucleus ^{7}Li. The breakup threshold of ^{6}Li into α-d is 1.47 MeV, while that of ^{7}Li into α-t is 2.45 MeV. It appears that if the ^{6}Li-breakup component $\sigma_{\alpha\text{-}d}$ could be separately measured and subtracted from $\sigma_{\alpha\text{-incl}}$, then the centroid of the distribution $D_{\rm qel}$, including the remaining α contribution, would perhaps match with that of $D_{\rm fus}$ (CF).

VI. SUMMARY

The QEL scattering excitation function for the system ^{6}Li + ^{159}Tb has been measured at large backward angle, at energies around the Coulomb barrier, and the corresponding

barrier distribution has been extracted, both with and without the contribution of α particles. The experimental QEL scattering excitation function and the barrier distribution derived only from $Z = 3$ events have been compared with the coupled channels calculations using the code FRESCO. The coupling to the low-lying inelastic excited states of ^{159}Tb up to $11/2^+$ and to the resonant first excited state of ^{6}Li gives a reasonable description of the barrier distribution, but underpredicts the excitation function data at higher energies. The CRC calculations, including n-pickup channel in the coupling scheme, did not show any significant effect. The observed disagreement between theory and experiment might be attributed to the effects of the direct and sequential breakup of ^{6}Li, as well as some transfer channels not considered here. For inclusion of breakup in the coupled channels calculations, one needs to carry out continuum discretized coupled channels calculations.

The barrier distribution extracted from the measured QEL scattering excitation function was then compared with the distribution $D_{\rm fus}$, derived from the CF cross sections of Ref. [22]. The $D_{\rm fus}$ was also determined from the coupled channels calculated fusion cross sections. The experimental and calculated $D_{\rm fus}$ agree fairly well with each other. It is observed that the distribution $D_{\rm qel}$ obtained from the sum of elastic and inelastic scattering and n-stripping events is broader and the peak is shifted lower in energy compared to $D_{\rm fus}$. The observed result is consistent with Zagrebaev's interpretation [5] that the QEL barrier distribution obtained from (elastic+inelastic+transfer) cross sections represents the total reaction threshold distribution and not the fusion barrier distribution. The maximum of the distribution $D_{\rm qel}$, including the α-particles contribution, reasonably matches with the maximum of $D_{\rm fus}$, but is seen to be broadened compared to $D_{\rm fus}$ at higher energies. This broadening in fact led to a shift of the centroid of the distribution $D_{\rm qel}$, including α-particles, towards higher energy with respect to that of $D_{\rm fus}$. This is in contradiction to that reported for ^{7}Li + ^{159}Tb [21]. The shift in the centroid of $D_{\rm qel}$ compared to $D_{\rm fus}$ (CF) for ^{6}Li + ^{159}Tb is attributed to the significant breakup probability of the relatively weakly bound ^{6}Li nucleus into α and d, unlike the case of ^{7}Li. In future, similar simultaneous investigation of $D_{\rm fus}$ and $D_{\rm qel}$ in reactions induced by other weakly bound projectiles, like ^{9}Be seems interesting.

ACKNOWLEDGMENTS

The authors thank the pelletron staff at the BARC-TIFR Pelletron Facility, Mumbai, for providing a stable beam. We would also like to thank Mr. Sujib Chandra Chatterjee of Saha Institute of Nuclear Physics for technical support during the experiment. One of the authors, P.B., would like to thank the Council of Scientific & Industrial Research, India, for their financial support.

[1] K. Hagino and N. Rowley, Phys. Rev. C **69**, 054610 (2004).
[2] M. Dasgupta, D. J. Hinde, N. Rowley, and A. M. Stefanini, Annu. Rev. Nucl. Part. Sci. **48**, 401 (1998) and references therein.
[3] N. Rowley, G. R. Satchler, and P. H. Stelson, Phys. Lett. B **254**, 25 (1991).
[4] H. Timmers, J. R. Leigh, M. Dasgupta, D. J. Hinde, R. C. Lemmon, J. C. Mein, C. R. Morton, J. O. Newton, and N. Rowley, Nucl. Phys. A **584**, 190 (1995).
[5] V. I. Zagrebaev, Phys. Rev. C **78**, 047602 (2008).
[6] S. Mitsuoka, H. Ikezoe, K. Nishio, K. Tsuruta, S. C. Jeong, and Y. Watanabe, Phys. Rev. Lett. **99**, 182701 (2007).
[7] L. F. Canto, P. R. S. Gomes, R. Donangelo, and M. S. Hussein, Phys. Rep. **424**, 1 (2006), and references therein.
[8] C. J. Lin, H. Q. Zhang, F. Yang, M. Ruan, Z. H. Liu, Y. W. Wu, X. K. Wu, P. Zhou, C. L. Zhang, G. L. Zhang, G. P. An, H. M. Jia, and X. X. Xu, Nucl. Phys. A **787**, 281 (2007).
[9] D. Patel, S. Mukherjee, B. K. Nayak, S. V. Suryanarayana, D. C. Biswas, E. T. Mirgule, Y. K. Gupta, L. S. Danu, B. V. John, and A. Saxena, Phys. Rev. C **89**, 064614 (2014).
[10] D. S. Monteiro, O. A. Capurro, A. Arazi, J. O. F. Niello, J. M. Figueira, G. V. Martí, D. M. Heimann, A. E. Negri, A. J. Pacheco, V. Guimarães, D. R. Otomar, J. Lubian, and P. R. S. Gomes, Phys. Rev. C **79**, 014601 (2009).
[11] S. Mukherjee, B. K. Nayak, D. S. Monteiro, J. Lubian, P. R. S. Gomes, S. Appannababu, and R. K. Choudhury, Phys. Rev. C **80**, 014607 (2009).
[12] D. R. Otomar, J. Lubian, P. R. S. Gomes, D. S. Monteiro, O. A. Capurro, A. Arazi, J. O. Fernández Niello, J. M. Figueira, G. V. Martí, D. Martínez Heimann, A. E. Negri, A. J. Pacheco, V. Guimarães, and L. C. Chamon, Phys. Rev. C **80**, 034614 (2009).
[13] K. Zerva, N. Patronis, A. Pakou, N. Alamanos, X. Aslanoglou, D. Filipescu, T. Glodariu, M. Kokkoris, M. La Commara, A. Lagoyannis, M. Mazzocco, N. G. Nicolis, D. Pierroutsakou, M. Romoli, and K. Rusek, Phys. Rev. C **80**, 017601 (2009).
[14] K. Zerva, A. Pakou, K. Rusek, N. Patronis, N. Alamanos, X. Aslanoglou, D. Filipescu, T. Glodariu, N. Keeley, M. Kokkoris, M. La Commara, A. Lagoyannis, M. Mazzocco, N. G. Nicolis, D. Pierroutsakou, and M. Romoli, Phys. Rev. C **82**, 044607 (2010).
[15] H. M. Jia, C. J. Lin, H. Q. Zhang, Z. H. Liu, N. Yu, F. Yang, F. Jia, X. X. Xu, Z. D. Wu, S. T. Zhang, and C. L. Bai, Phys. Rev. C **82**, 027602 (2010).
[16] K. Zerva, A. Pakou, N. Patronis, P. Figuera, A. Musumarra, A. Di Pietro, M. Fisichella, T. Glodariu, M. La Commara, M. Lattuada, M. Mazzocco, M. G. Pellegriti, D. Pierroutsakou, A. M. Sanchez-Benitez, V. Scuderi, E. Strano, and E. Rusek, Eur. Phys. J. A **48**, 102 (2012).
[17] M. Zadro, P. Figuera, A. Di Pietro, M. Fisichella, M. Lattuada, T. Lönnroth, M. Milin, V. Ostashko, M. G. Pellegriti, V. Scuderi, D. Stanko, E. Strano, and D. Torresi, Phys. Rev. C **87**, 054606 (2013).
[18] C. S. Palshetkar, Shital Thakur, V. Nanal, A. Shrivastava, N. Dokania, V. Singh, V. V. Parkar, P. C. Rout, R. Palit, R. G. Pillay, S. Bhattacharyya, A. Chatterjee, S. Santra,

K. Ramachandran, and N. L. Singh, Phys. Rev. C **89**, 024607 (2014).
[19] M. M. Shaikh, Subinit Roy, S. Rajbanshi, M. K. Pradhan, A. Mukherjee, P. Basu, S. Pal, V. Nanal, R. G. Pillay, and A. Shrivastava, Phys. Rev. C **91**, 034615 (2015).
[20] M. M. Shaikh, Subinit Roy, A. Mukherjee, A. Goswami, Balaram Dey, S. Pal, S. Roy, A. Shrivastava, S. K. Pandit, and K. Mahata, Phys. Rev. C **102**, 024627 (2020).
[21] P. Biswas, A. Mukherjee, D. Chattopadhyay, Saikat Bhattacharjee, M. K. Pradhan, M. M. Shaikh, Subinit Roy, A. Goswami, P. Basu, S. Santra, S. K. Pandit, K. Mahata, and A. Shrivastava, Phys. Rev. C **103**, 014606 (2021).
[22] M. K. Pradhan, A. Mukherjee, P. Basu, A. Goswami, R. Kshetri, R. Palit, V. V. Parkar, M. Ray, S. Roy, P. R. Chowdhury, M. S. Sarkar, and S. Santra, Phys. Rev. C **83**, 064606 (2011).
[23] Computer code LAMPS (Linux Advanced Multiparameter System), http://www.tifr.res.in/~pell/lamps.html
[24] A. Shrivastava, A. Navin, N. Keeley, K. Mahata, K. Ramachandran, V. Nanal, V. V. Parkar, A. Chatterjee, and S. Kailas, Phys. Lett. B **633**, 463 (2006).
[25] D. H. Luong, M. Dasgupta, D. J. Hinde, R. du Rietz, R. Rafiei, C. J. Lin, M. Evers, and A. Diaz-Torres, Phys. Rev. C **88**, 034609 (2013).
[26] M. K. Pradhan, A. Mukherjee, Subinit Roy, P. Basu, A. Goswami, R. Kshetri, R. Palit, V. V. Parkar, M. Ray, M. Saha Sarkar, and S. Santra, Phys. Rev. C **88**, 064603 (2013).
[27] P. J. A. Buttle and L. J. B. Goldfarb, Nucl. Phys. A **176**, 299 (1971).
[28] S. Santra, S. Kailas, V. V. Parkar, K. Ramachandran, V. Jha, A. Chatterjee, P. K. Rath, and A. Parihari, Phys. Rev. C **85**, 014612 (2012).
[29] O. A. Capurro, A. J. Pacheco, A. Arazi, J. M. Figueira, D. Martinez Heimann, A. E. Negri, Nucl. Phys. A **849**, 1 (2011).
[30] A. Gavron, Phys. Rev. C **21**, 230 (1980).
[31] I. J. Thompson, Comput. Phys. Rep. **7**, 167 (1988).
[32] G. R. Satchler and W. G. Love, Phys. Rep. **55**, 183 (1979).
[33] D. T. Khoa and W. von Oertzen, Phys. Lett. B **304**, 8 (1993); D. T. Khoa, W. von Oertzen, and H. G. Bohlen, Phys. Rev. C **49**, 1652 (1994).
[34] http://www-nds.iaea.org/RIPL-2
[35] http://www.nndc.bnl.gov
[36] F. Eigenbrod, Z. Phys. **228**, 337 (1969).
[37] J. Cook, Nucl. Phys. A **388**, 153 (1982).
[38] T. Y. Li and S. K. Mark, Nucl. Phys. A **123**, 147 (1969).
[39] F. D. Becchetti, Jr. and G. W. Greenlees, Phys. Rev. **182**, 1190 (1969).
[40] A. A. Rudchik, A. T. Rudchik, G. M. Kozeratska, O. A. Ponkratenko, E. I. Koshchy, A. Budzanowski, B. Czech, S. Kliczewski, R. Siudak, I. Skwirczyńska, A. Szczurek, S. Yu. Mezhevych, K. W. Kemper, J. Choiński, T. Czosnyka, and L. Glowacka, Phys. Rev. C **72**, 034608 (2005).
[41] C. Beck, N. Keeley, and A. Diaz-Torres, Phys. Rev. C **75**, 054605 (2007).
[42] D. H. Luong, M. Dasgupta, D. J. Hinde, R. du Rietz, R. Rafiei, C. J. Lin, M. Evers, and A. Diaz-Torres, Phys. Lett. B **695**, 105 (2011).
[43] M. K. Pradhan, Ph.D. thesis, University of Calcutta, 2011.
[44] K. Hagino, N. Rowley, and A. T. Kruppa, Comput. Phys. Commun. **123**, 143 (1999).
[45] D. S. Monteiro, P. R. S. Gomes, and J. Lubian, Phys. Rev. C **80**, 047602 (2009).